Elasticity, Strength, and Water Permeability of Bilayers that Contain Raft Microdomain-Forming Lipids

W. Rawicz,* B. A. Smith,* T. J. McIntosh,† S. A. Simon,‡ and E. Evans*§

*Department of Physics and Department of Pathology, University of British Columbia, Vancouver, Canada; †Department of Cell Biology and ‡Department of Neurobiology, Duke University Medical Center, Durham, North Carolina 27710; and §Biomedical Engineering, Boston University, Boston, Massachusetts 02215

ABSTRACT Bilayers composed of phosphatidylcholine (PC), sphingomyelin (SM), and cholesterol (CHOL) are commonly used as systems to model the raft-lipid domain structure believed to compartmentalize particular cell membrane proteins. In this work, micropipette aspiration of giant unilamellar vesicles was used to test the elasticities, water permeabilities, and rupture tensions of single-component PC, binary 1:1 PC/CHOL, and 1:1 SM/CHOL, and ternary 1:1:1 PC/SM/CHOL bilayers, one set of measurements with dioleoyl PC (DOPC; C18:1/C18:1 PC) and the other with stearoyloleoyl PC (SOPC; C18:0/C18:1 PC). Defining the elastic moduli (K_A), the initial slopes of the increase in tension (σ) versus stretch in lipid surface area (α_e) were determined for all systems at low (15°C) and high (32–33°C) temperatures. The moduli for the single-component PC and binary phospholipid/CHOL bilayers followed a descending hierarchy of stretch resistance with SM/CHOL > SOPC/CHOL > DOPC/CHOL > PC. Although much more resistant to stretch than the single-component PC bilayers, the elastic response of vesicle bilayers made from the ternary phospholipid/CHOL mixtures showed an abrupt softening (discontinuity in slope), when immediately subjected to a steady ramp of tension at the low temperature (15°C). However, the discontinuities in elastic stretch resistance at low temperature vanished when the bilayers were held at ~1 mN/m prestress for long times before a tension ramp and when tested at the higher temperature 32–33°C. The elastic moduli of single-component PC and DOPC/CHOL bilayers changed very little with temperature, whereas the moduli of the binary SOPC/CHOL and SM/CHOL bilayers diminished markedly with increase in temperature, as did the ternary SOPC/SM/CHOL system. For all systems, increasing temperature increased the water permeability but decreased rupture tension. Concomitantly, the measurements of permeability exhibited a prominent correlation with the rupture tension across all the systems. Together, these micromechanical tests of binary and ternary phospholipid/CHOL bilayers demonstrate that PC hydrocarbon chain unsaturation and temperature are major determinants of the mechanical and permeation properties of membranes composed of raft microdomain-forming lipids.

INTRODUCTION

The outer membranes of eukaryotic cells typically contain higher concentrations of cholesterol (CHOL) and sphingomyelin (SM) than do internal membranous organelles (1,2). For example, along the secretion pathway, the concentrations of CHOL and sphingolipids increase from the endoplasmic reticulum through the Golgi apparatus to the plasma membrane (1,3). These trans-Golgi and plasma membranes are thought to contain lateral microdomains, termed ''rafts'' (4–7), that are enriched in CHOL and SM (2,8,9). Although some membrane proteins are excluded from rafts (10), other types of proteins appear to be associated with rafts, including acylated proteins (11–13), glycosyl-phosphatidylinositol-anchored proteins (14,15), and certain transmembrane receptors (16,17) and ion channels (18–20). Due to their ability to sequester specific lipids and proteins, rafts are thought to be involved in a number of important cell functions, including signal transduction (13,21), lipid sorting (5,22,23), and protein trafficking (4,24). Specifically, an early fundamental question related to lipid and protein sorting was whether rafts would form in lipid mixtures in the absence of proteins. For example, in the Golgi apparatus, Simons and van Meer (22) envisaged a lateral separation of glycerolipids and sphingolipids as the necessary first event in the sorting process. In the past several years, many experimental studies have shown that raft microdomains do form in lipid bilayers for lipid compositions approximating those found in trans-Golgi or plasma membranes. Along with structural characterization by x-ray diffraction (9), a variety of techniques, including fluorescent probes (8), atomic force microscopy (25), and light microscopy (26–29), have been used to image microdomains in bilayers composed of a combination of an unsaturated phosphatidylcholine (PC), SM, and CHOL. For dioleoyl phosphatidylcholine (DOPC)/SM/CHOL model systems, the nonraft domains appear to be enriched in the unsaturated DOPC, whereas the raft domains are enriched in SM and CHOL (9,28).

Another key factor thought to be important in the sorting of transmembrane peptides or proteins is the difference in elastic deformabilities between raft and nonraft bilayers (30–32). Due to the high concentrations of CHOL and SM with its long hydrocarbon chains, raft-lipid bilayers are expected to be much less compressible in area than PC/CHOL bilayers. Indeed, previous tests of the area-stretch moduli (K_A) for SM/CHOL bilayers at room temperature have produced

Submitted September 10, 2007, and accepted for publication February 21, 2008.

Lead authors W. Rawicz and B. A. Smith contributed equally to this work.

Address reprint requests to E. Evans, E-mail: evans@physics.ubc.ca.

Editor: Peter Tieleman.

0006-3495/08/06/4725/12 $2.00

doi: 10.1529/biophysj.107.121731

values 10-fold larger than that of a typical single-component PC (nonraft) bilayer (33–35). However, little is known about how the elastic properties of SM/CHOL and PC/SM/CHOL bilayers change as temperatures approach physiological conditions. The temperature dependence of elasticity for raft-containing bilayers is of interest because previous studies have shown that the size and shape of rafts (26–28), as well as the sorting of lipids and transmembrane peptides (31,32), depend on temperature. Significantly, microdomains are often not resolvable in PC/SM/CHOL bilayers by light microscopy at temperatures above 30°C (26–28). Moreover, even less is known about how temperature affects the mechanical strength and permeability properties of bilayers containing both raft and nonraft microdomains and to what extent lateral phase separation of membrane lipids may modulate bilayer strength and permeability, both critical to plasma membrane function.

In this work, we present results from micromechanical experiments on giant bilayer vesicles that demonstrate the impact of temperature on the elastic area-stretch moduli (K_A), rupture (lysis) tensions (σ_L), and water permeabilities (P_W) of bilayers containing PC, binary PC/CHOL and SM/CHOL, and ternary PC/SM/CHOL. Based on published data, the 1:1:1 ternary systems tested in our experiments at low temperature (15°C) are expected to contain microdomains, whereas the PC and binary PC/CHOL systems are not. Consistent with the most commonly studied raft microdomain-containing bilayer systems (36), one set of measurements was performed using vesicle bilayers that contained the symmetrically unsaturated DOPC ((C18:1) (C18:1) PC). We also tested bilayer systems that contained stearoyloleoyl phosphatidylcholine (SOPC) ((C18:0) (18:1) PC) to compare how symmetric and asymmetric acyl chain unsaturation affect the mechanical and permeability properties of bilayers as well as their change with temperature. PC acyl-chain saturation is an important consideration in biological membranes since glycerophospholipids in plasma membranes normally contain a saturated chain in the *sn*-1 position (3), and adding a double bond is known to dramatically change phospholipid-phospholipid and phospholipid-CHOL interactions as well as in the lateral organization of bilayer domains (28,37). Consistent with these features, we show that PC acyl-chain saturation has a major effect on material properties of bilayers containing CHOL. Yet, these measurements also demonstrate that interactions with CHOL are an important factor in the properties of bilayers containing DOPC.

MATERIALS AND METHODS

Materials

Brain SM, DOPC, SOPC, and CHOL were purchased from Avanti Polar Lipids (Alabaster, AL) and used without further purification. The gel to liquid crystalline phase transitions are ~40°C (broad), 6°C, and −20°C for SM, SOPC, and DOPC, respectively ((34) and Avanti Polar Lipids catalog).

Vesicle preparation

Giant unilamellar vesicles (GUVs) were formed by slow hydration of lipid films as described previously (35,38). The lipid mixtures were first dissolved in chloroform (10 mg/ml). Then 20–30 μl of the lipid solution was spread on a roughened Teflon disk, followed by evaporation of the chloroform for >4 h in a vacuum chamber. Next, the dried lipid film was prehydrated by passing warm water vapor over the disk for 10 min, which was carried by argon gas after perfusion through distilled water at 35–40°C. The final swelling step used to form the GUVs involved soaking the disk in 200 mM sucrose overnight at 37°C for PC or mixed PC/CHOL films and at >50°C for lipid films containing SM. Before the micropipette tests, the vesicle suspension was equilibrated at room temperature for 2–3 h. Then an aliquot of the vesicle suspension was diluted manyfold in a buffer containing glucose with an osmolarity 2–5 mOsm/kg higher than the sucrose solution used for swelling. The difference of inside-outside solutions created a refractive index and density gradient across the vesicle membrane, providing excellent image contrast and sedimentation of the vesicles to the bottom of the chamber.

Measurements of bilayer elasticity, strength, and water permeability

Selected from a very dilute suspension, individual GUVs were captured by a micropipette with a suction pressure that set the initial membrane tension in the range of 0.5–1 mN/m. At this level of tension, all vesicles were pulled tightly into the pipette, exhibiting an optically perfect spherical shape outside the pipette. To prevent necking of the aspirated projection inside the pipette under the large suctions needed to stretch the vesicle surface, the initial projection length was limited to 1.5–2 pipette diameters by slight adjustment of the outside osmolarity of the vesicle suspension before injection into the microscope chamber. Once captured, a vesicle was then either stressed by steadily increasing the pipette suction to determine the elastic stretch modulus (K_A) and rupture (lysis) tension (σ_L) or held at constant tension and transferred to an adjacent chamber with higher osmolarity to determine the coefficient of bilayer permeability to water (P_w), following procedures developed in our other studies (35,38–40). To set and maintain the temperature, a circulating temperature-controlled water system was plumbed to a heat-exchange jacket that formed one wall of the test chamber. A tiny thermocouple was placed near the site of vesicle tests in the chamber to control the temperature (within 0.5°C).

Stretch elasticity

Immediately after initial capture or after an extended period of prestress, vesicles were steadily pressurized at a rate set to apply a 2 mN/m/s ramp of tension to test the bilayer area elasticity and strength. To quantify the change in surface area under the increasing tension $\sigma(t)$, the length of the vesicle projection pulled into the micropipette and the length of the vesicle spherical shape outside the pipette were tracked using high-resolution image analysis (40,41). At the levels of tension needed to expand the bilayer-surface area, the pipette suctions applied to the ~20 μm vesicles were small (~10^3 Pa) in comparison to the osmotic activity of the trapped sucrose (~5×10^5 Pa) and insufficient to draw water out of a vesicle during the short time frame of an elasticity and rupture test. Thus, the vesicle volume could be treated as effectively fixed during the area expansion test, allowing the change in visible area ($\Delta A/A_o$) of the vesicle to be accurately computed from the increase in projection length inside the pipette. Even so, to determine the bilayer stretch modulus (K_A), it was necessary to quantify the dilation in lipid-surface area α_e under the increasing tension $\sigma(t)$.

As demonstrated previously (35,39), the apparent geometric increase in vesicle-surface area $\Delta A/A_o$ measured optically includes the elastic stretch of the lipid surface α_e plus a small (submicroscopic) expansion in area $\alpha_{\approx}$ contributed by reduction in thermal-bending undulations, i.e., $\Delta A/A_o = \alpha_e + \alpha_{\approx}$. To determine the direct stretch in lipid-surface area $\alpha_e = \Delta A/A_o - \alpha_{\approx}$,

the reduction in thermal undulations at each tension was subtracted from the apparent area expansion using the compliance relation established previously, $\alpha_{\approx} = (k_B T/8\pi k_c)\log_e(\sigma/\sigma_o)$, which is governed by the ratio of thermal energy $k_B T$ to the bilayer bending modulus k_c (35,39). In the case of the single-component lipid and binary phospholipid/CHOL bilayers, the values for elastic-bending moduli were taken from previous measurements. Although almost negligible in the case of the ternary PC/SM/CHOL bilayers, the small contributions from thermal undulations to the area expansions in vesicles were treated the same way, using approximate bending moduli estimated by interpolation between the properties of the binary phospholipid/CHOL systems.

Rupture strength

In the course of testing bilayer stretch elasticity, the strength of each bilayer was quantified by the value of tension σ_L at the instant (within 1 ms) of vesicle lysis, as indicated by each ''star'' (*) in Fig. 1. To provide a simple

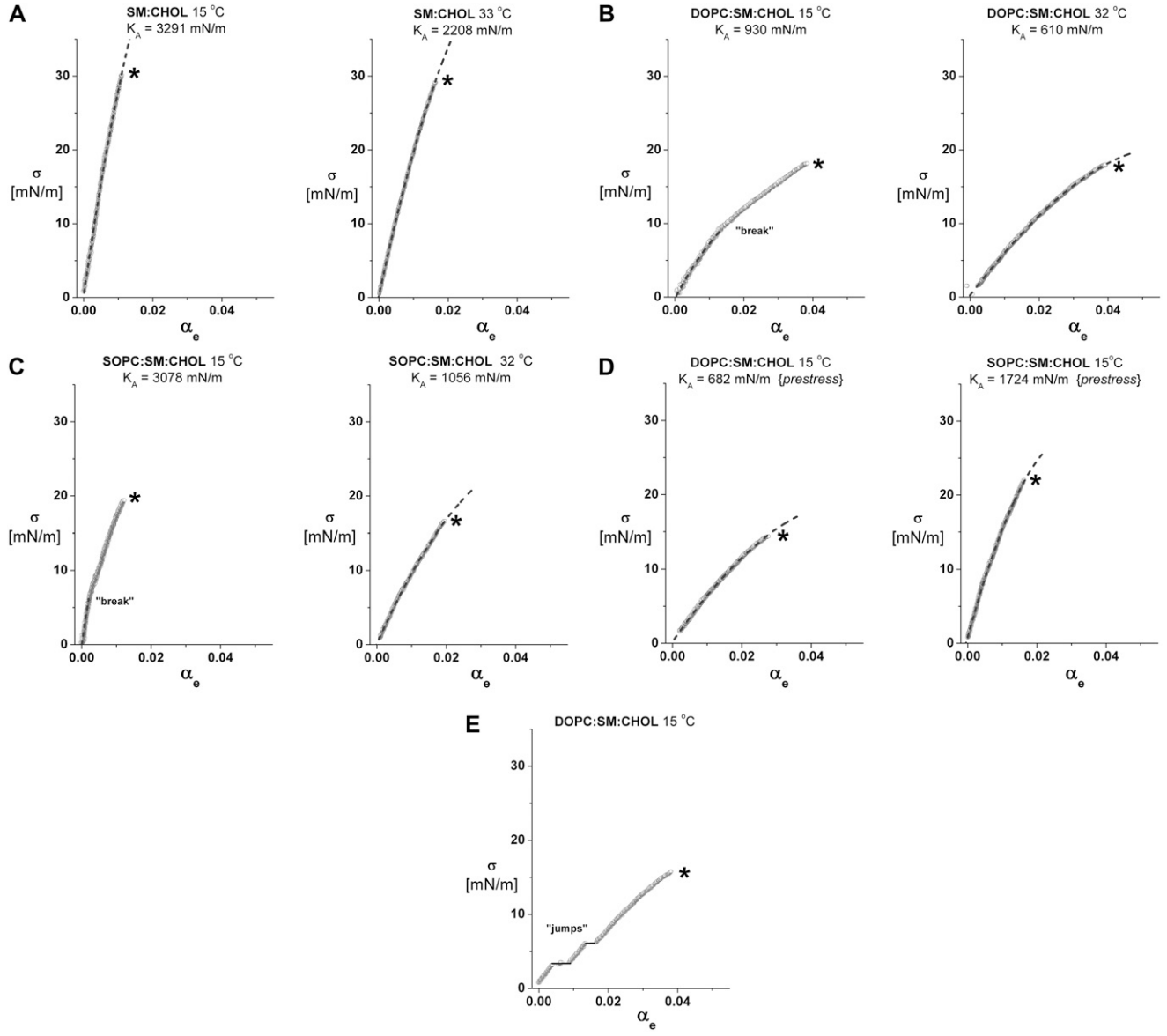

FIGURE 1 Representative examples of vesicle bilayer tension σ versus dilation in lipid-surface area α_e measured by micropipette pressurization at 15°C and at 32–33°C. (To emphasize the data, the ~1000 points measured during each test are plotted as small gray circles. The dotted black curves superposed on the data are fits of a cubic polynomial used to accurately determine the slope at zero tension (e.g., the elastic modulus K_A) as discussed in the text. (*A*) Sample tests of 1:1 SM/CHOL vesicles show the smooth-continuous stretch response seen at both 15°C (*left panel*) and 33°C (*right panel*). (*B*) Tests of 1:1:1 DOPC/SM/CHOL vesicles loaded continuously without prestress (see text) show a break in slope near 10 mN/m observed routinely at 15°C (*left panel*) and the smooth-continuous stretch response observed at 32°C (*right panel*). (*C*) As for the DOPC/SM/CHOL system, tests of 1:1:1 SOPC/SM/CHOL vesicles loaded continuously without prestress show a break in slope near 5 mN/m observed routinely at 15°C (*left panel*) and a smooth-continuous stretch response at 32°C (*right panel*). (*D*) On the other hand, tests of 1:1:1 DOPC/SM/CHOL vesicles (*left panel*) and 1:1:1 SOPC/SM/CHOL (*right panel*) vesicles show the smooth-continuous stretch response observed routinely at 15°C when subjected to prestress followed by continuous loading. (*E*) Only rarely seen (<10% of cases), this test of a 1:1:1 DOPC/SM/CHOL vesicle at 15°C shows discrete jumps in area presumably due to incorporation of fluid membrane blebs.

comparison among the strength measurements reported here, the values of lysis tension σ_L were obtained at a single tension (ramp) rate of 2 mN/m/s. Even though rupture strength depends on the ramp rate (40,42), the lysis tensions vary weakly with stress rate below 10 mN/m/s (see detailed treatment in the Appendix).

Water permeability

To measure the coefficient of bilayer permeability to water, single vesicles were selected by a micropipette and then transferred to an adjacent microscope chamber with ~15% higher osmolarity where the time course of dehydration was analyzed as described previously (38). The transfer process involved passing the vesicle through a small air gap that separated the microscope chambers. To do this, the vesicle was held by a micropipette and inserted into the entrance of a much larger pipette. The microscope stage was then translated to leave the sequestered vesicle in the second chamber, where it was exposed to the new osmotic environment. Typically, vesicles were transferred from a chamber that contained 200 mOsm glucose to a chamber that contained ~230 mOsm glucose. Consistent with passive osmotic transport, we have previously shown (38) that higher or lower osmolarities yield linearly proportional faster or slower filtration rates with the same coefficient for water permeability. Moreover, transfer back to the original chamber recovers the original vesicle volume, showing no loss of vesicle sucrose or uptake of outside glucose (38).

Throughout each test, the vesicle was held under small, fixed suction pressure, setting a low bilayer tension (~1 mN/m). The changes in vesicle volume were computed from the time-dependent increase in the aspirated projection length. The time course of volume change was analyzed to obtain the rate of filtration, using the standard phenomenological law for water transport across a semipermeable membrane (43). The change of vesicle volume in time is proportional to the surface area A, the coefficient for water permeability P_w, and the outside-inside difference in mole fraction of solute, $\Delta x_s(t) = x_{s_\infty} - x_s(t)$, as given by $dV/dt = -AP_w\Delta x_s$. Impermeable to solutes (on the timescale for water filtration), the solute mole fraction inside the vesicle (or equivalently the osmolarity, x_s/v_w, when scaled by the molar volume of water v_w) varies in inverse proportion to the volume given the fixed number of moles m of trapped solute, i.e., $x_s = v_w m/V(t)$. Integration of the transport relation predicts that the relative vesicle volume, $\bar{V}(t) = V(t)/V(o)$, follows transcendental expression:

$$k_w t = r_{osm}[1 - \bar{V}(t)] + \ln[(r_{osm} - 1)/(r_{osm}\bar{V}(t) - 1)],$$

which is parameterized by the ratio of final/initial osmolarities $r_{osm} = x_{s_\infty}/x_{so}$ and the filtration rate $k_w = AP_w[r_{osm}x_{s_\infty}/V(o)]$. As shown by the example in Fig. 4 *A*, the fit of this transport model to the reduction in vesicle volume yields the filtration rate k_w, which is then converted to the permeability coefficient using the vesicle area A, initial volume $V(o)$, and solution osmolarities (38).

X-ray diffraction

The bilayer thicknesses of 1:1 SOPC/CHOL and 1:1:1 SOPC/SM/CHOL were determined by techniques previously used for DOPC, 2:1 DOPC/CHOL, 1:1 SM/CHOL, 1:1:1 DOPC/SM/CHOL, and SOPC (9,34,35). In brief, oriented multibilayers were deposited on a curved glass surface by evaporation from chloroform. The supported multibilayers were mounted in a controlled humidity chamber of a line-focused x-ray camera. The lamellar diffraction was recorded and analyzed as described previously (9,34,35).

RESULTS

Bilayer lipid-area elasticity

Fig. 1, *A–D*, shows particular examples of vesicle tension σ versus lipid-area dilation α_e obtained at 15°C and 32–33°C for bilayers composed of 1:1 SM/CHOL, 1:1:1 DOPC/SM/CHOL, and 1:1:1 SOPC/SM/CHOL. As detailed below, these sample data demonstrate the significant impact of composition and temperature on the elastic response and rupture strength of SM/CHOL-containing bilayers and how the properties of these bilayers depended on whether or not the vesicles were subjected to prestress. Ramped at a tension rate of 2 mN/m/s, each vesicle membrane was stretched until lysis; the rupture strength was quantified by the level of tension (σ_L) at the maximum area stretch (marked by the last data point adjacent to the symbol *). In these plots, the small gray circles represent the measurements (σ, α_e), and the dotted black lines are fits of a cubic polynomial in the lipid area strain where the coefficient of the linear term was used to define the elastic modulus K_A at zero tension. The pronounced differences of elastic moduli in phospholipid/CHOL systems are clearly seen in Fig. 1, *A–D*, following a descending order given by SM/CHOL > SOPC/SM/CHOL > DOPC/SM/CHOL.

As shown by the examples in the left panels of Fig. 1, *B* and *C*, abrupt downward shifts (discontinuous ''breaks'') in the slope appeared in the tension σ versus lipid-area dilation α_e responses of the ternary 1:1:1 DOPC/SM/CHOL and SOPC/SM/CHOL vesicles at 15°C when subjected to a ramp of tension from an initially unstressed state. However, the breaks were not observed in any of the vesicle systems at 32–33°C (*right-hand panels* of Fig. 1, *B* and *C*). Importantly, prestressing the ternary lipid/CHOL vesicles at 15°C with ~1 mN/m for long times (>1 min) eliminated the breaks in slope, leaving the smooth elastic responses illustrated in Fig. 1 *D* and those observed routinely at high temperature. In the absence of prestress, the discontinuity in elastic response at 15°C appeared at ~9 mN/m for the DOPC-containing vesicles and at ~4–5 mN/m for the SOPC-containing vesicles. Before the breaks in slope, the bilayers were much more resistant to change in area (e.g., $\Delta\sigma/\Delta\alpha_e \sim 900$ mN/m for DOPC/SM/CHOL and ~2200 mN/m for SOPC/SM/CHOL) than following the breaks (e.g., $\Delta\sigma/\Delta\alpha_e \sim 650$ mN/m for DOPC/SM/CHOL and ~1720 mN/m for SOPC/SM/CHOL). Moreover, the slopes of the elastic response following breaks were consistent with the elastic area compressibility measured after prolonged periods of prestress (Fig. 2).

The appearance of discontinuities in elastic response of these ternary bilayers at 15°C suggests that some type of inhomogeneous structure was initially present in the materials. The subsequent elimination of the discontinuities in elasticity by large tensions or by prior periods of prestress indicates that the mechanical stress acted to break up the inhomogeneities. Note that for all the bilayer systems at both temperatures, a few vesicles (<10% of cases) exhibited small discrete jumps in apparent area (Fig. 1 *E*) once they became dehydrated after long periods in the microscope chamber. Although usually not detected in the optical images, the jumps in apparent area were most likely due to incorporation

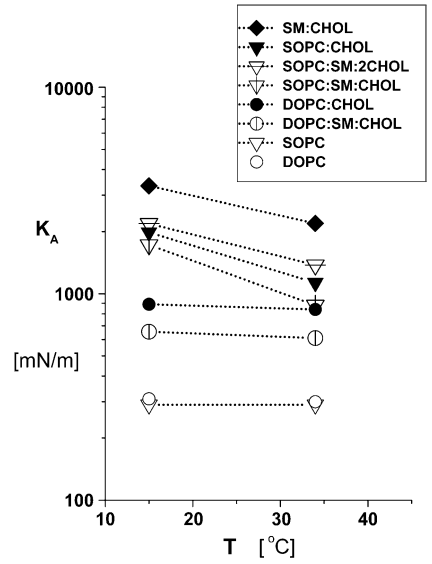

FIGURE 2 Average lipid area-stretch moduli K_A measured at 15°C and 32–33°C for SOPC, 1:1 DOPC/CHOL, 1:1 SOPC/CHOL, 1:1 SM/CHOL, 1:1:1 DOPC/SM/CHOL, and 1:1:1 SOPC/SM/CHOL bilayers. Fifty to eighty vesicles were tested for each system and temperature (means ± SD given in Table 1). The elastic moduli for the ternary 1:1:1 DOPC/SM/CHOL and 1:1:1 SOPC/SM/CHOL systems at 15°C represent vesicles subjected to prestress followed by continuous loading (Fig. 1). Also plotted for comparison as discussed in the text are results for 1:1:2 SOPC/SM/CHOL vesicles.

of small membrane blebs. Prestressing the vesicles at ~1 mN/m for long times was found to eliminate the area jumps.

The elastic moduli (K_A) derived from the area-stretch responses of the prestressed vesicles are listed in Table 1 and plotted in Fig. 2, demonstrating that the addition of CHOL to bilayers made with both SOPC and DOPC markedly increases their resistance to area stretch. For example, the addition of 50 mol % CHOL to SOPC bilayers produced a sixfold increase in elastic modulus from K_A ~290 mN/m to ~1980 mN/m at 15°C, and adding 50 mol % CHOL to DOPC bilayers produced a nearly threefold increase in the modulus from K_A ~300 mN/m to ~890 mN/m at 15°C. Still larger values were obtained for 1:1 SM/CHOL vesicles, reaching K_A ~3320 mN/m at 15°C. Moreover, diluting the ratio of CHOL to phospholipid in 1:1 PC/CHOL bilayers by addition of SM reduced the elastic moduli, as shown by the results for vesicles made with 1:1:1 PC/SM/CHOL. On the other hand, concomitant to the increase of acyl chain interactions with CHOL, increasing the fraction of CHOL from 1:1:1 to 1:1:2 in SOPC/SM/CHOL bilayers produced even larger values for the elastic moduli than the moduli of the binary SOPC/CHOL vesicles (Table 1). Significantly, as seen in Fig. 2, increasing temperature from 15°C to 32–35°C reduced the elastic moduli of the SOPC/CHOL, SOPC/SM/CHOL, and SM/CHOL bilayers by ~50%. However, the elastic moduli of DOPC/CHOL and prestressed DOPC/SM/CHOL bilayers were little affected by the increase in temperature.

Rupture tension

Listed in Table 1 and plotted in Fig. 3 *A*, the strengths of PC bilayers were found to increase significantly with the incorporation of CHOL. For example, at 15°C, σ_L increased from ~12 mN/m for SOPC to ~26 mN/m for 1:1 SOPC/CHOL and from ~10 mN/m for DOPC to ~19 mN/m for 1:1 DOPC/CHOL. The values of rupture tensions decreased with increasing temperature for all of the phospholipid/CHOL systems. Of the mixed systems, the strongest vesicles at both low and high temperatures were clearly the SM/CHOL vesicles (e.g., ~33 mN/m at 15°C), followed by SOPC/CHOL then DOPC/CHOL. Likewise, bilayers made from the 1:1:1 ternary systems with SOPC/SM/CHOL were much stronger (~21 mN/m at 15°C) than those containing DOPC/SM/CHOL (~15 mN/m at 15°C). Paralleling the effect of increased CHOL content on elastic moduli, the rupture tensions for 1:1:2 SOPC/SM/CHOL vesicles were larger than those of 1:1:1 SOPC/SM/CHOL vesicles, exhibiting strengths comparable to 1:1 SOPC/CHOL vesicles.

Even though the membrane strengths plotted in Fig. 3 *A* represent loading at one stress rate $\Delta\sigma/\Delta t$ ($r_\sigma = 2$ mN/m/s), rupture tensions were measured at three or more stress rates spanning a range from 0.05 to > 50 mN/m/s for all phospholipid/CHOL vesicle systems (see data in the Appendix). Between 0.05 and 5 mN/m/s, the lysis tensions σ_L exhibited weak stress-rate dependences, increasing by only 20%–25%. Shown in the Appendix for phospholipid/CHOL systems, and previously for fluid PC bilayers with chain lengths from 13 to 22 carbons (40), the weak stress-rate regime follows a transcendental relation predicted by a kinetic theory for hole nucleation in tense fluid films (40,42), i.e., $\sigma_\beta/\sigma_L \approx (5/2)\log_e(\sigma_L/\sigma_\beta) - \log_e[(r_\sigma/(\nu_h^o\sigma_\beta)]$. The weak stress-rate dependence arises from a reciprocal dependence on tension in the Arrhenius factor, i.e., $\exp(-\sigma_\beta/\sigma)$, which characterizes the kinetic frequency of failure ν_{rup}(1/time) under stress. Relatively insensitive to the frequency-scale prefactor ν_h^o, the principal parameter determining membrane strength is the thermal tension scale σ_β derived from the ratio of the activation energy to the thermal energy k_BT. The thermal tension scale characterizes the magnitude of the energy barrier that impedes the opening of an unstable hole and its susceptibility to the application of membrane stress (see Appendix). Supporting the validity of a single stress-rate assay at 2 mN/m/s, the lysis tensions obtained at 15°C are shown in Fig. 3 *B* to correlate closely with the values of σ_β obtained from fitting the kinetic model for rupture to the stress-rate dependence of the measurements. As shown by the values in Fig. 3 *B*, the rupture tensions at 2 mN/m/s were a small fraction (~0.1) of the tension scales σ_β for all systems, demonstrating the enormity of the activation barriers that sustain membrane cohesion.

TABLE 1 Elasticity, strength, and water permeability measurements

	$K_A \pm$ SD (mN/m)		$\sigma_{Lysis} \pm$ SD (mN/m)		$P_w \pm$ SD (μm/s)		
System	15°C	32–35°C	15°C	32–35°C	15°C	30°C	35°C
One component							
DOPC	310 ± 20	—	10 ± 3	—	25.9 ± 3.1	56 ± 9	70 ± 6
SOPC	290 ± 6	290 ± 17	12 ± 3	—	19.7 ± 3.3	34 ± 7	44.6 ± 6
1:1 Binary							
DOPC/CHOL	890 ± 64	870 ± 141	19 ± 4	16 ± 2	5.8 ± 0.6	—	—
SOPC/CHOL	1985 ± 330	1130 ± 110	26 ± 3	21 ± 3	1.5 ± 0.2	6.4 ± 1.3	12.3 ± 3
SM/CHOL	3327 ± 276	2193 ± 209	33 ± 4	26 ± 5	0.36 ± 0.1	3.9 ± 1	5.9 ± 2
1:1:1 Ternary							
DOPC/SM/CHOL	655 ± 128	610 ± 61	15 ± 3	11.9 ± 3	3.4 ± 0.6	9.3 ± 1.2	19.1 ± 5
SOPC/SM/CHOL	1725 ± 300	880 ± 130	21.2 ± 3	16.7 ± 3	1.2 ± 0.1	4.3 ± 0.3	8.9 ± 1.4
1:1:2 Ternary							
SOPC/SM/CHOL	2188 ± 331	1377 ± 172	26 ± 3	—	1.5 ± 0.2	—	4.8 ± 0.8

Water permeability

Fig. 4 *A* shows an example of water filtration from a 1:1:1 SOPC/SM/CHOL vesicle after transfer to a hyperosmotic environment at 15°C. Water filtration across the CHOL-containing bilayers was very slow and thus unaffected by unstirred layers (38). Demonstrated by the curve superposed in Fig. 4 *A*, the integrated transport expression described in the Materials and Methods section was fit to each time course of vesicle dehydration by optimal choice of the filtration rate k_w. With the initial values for vesicle area, volume, and inside/outside solution osmolarities, the coefficient P_w for bilayer water permeability was computed from the filtration rate k_w using the equation given in the Materials and Methods section. The values of P_w measured at 15°C, 30°C, and 35°C are listed in Table 1 and plotted in Fig. 3 *B*, demonstrating the significant effect of temperature on bilayer transport properties. Also significant, the values for P_w exhibited a hierarchy spanning two orders of magnitude, with the largest being DOPC (~26 μm/s) > SOPC (~20 μm/s) > 1:1 DOPC/CHOL (~6 μm/s) > 1:1:1 DOPC/SM/CHOL (~3.4 μm/s) > 1:1 SOPC/CHOL (~1.5 μm/s) ≅ 1:1:1 SOPC/CHOL (~1 μm/s) > 1:1 SM/CHOL (0.4 μm/s) taking values at 15°C, which emphasizes the major impact of CHOL on bilayer permeability for all of the phospholipids.

DISCUSSION

Elasticity of bilayers that contain raft microdomain-forming lipids

The elastic stretch responses of bilayers containing a single-fluid phase PC or 1:1 binary mixtures of phospholipid/CHOL all followed smooth, slightly nonlinear tension versus lipid-area dilation relationships both at low (15°C) and high (32–35°C) temperatures. By comparison, abrupt downward breaks in the slope of this relationship were observed in the stretch responses of both 1:1:1 ternary PC/SM/CHOL systems at 15°C if not first subjected to long periods of prestress. Demonstrated by the left panels in Fig. 1, *B* and *C*, and described in the Results section, the slopes of the elastic stretch responses for unprestressed ternary lipid/CHOL vesicles

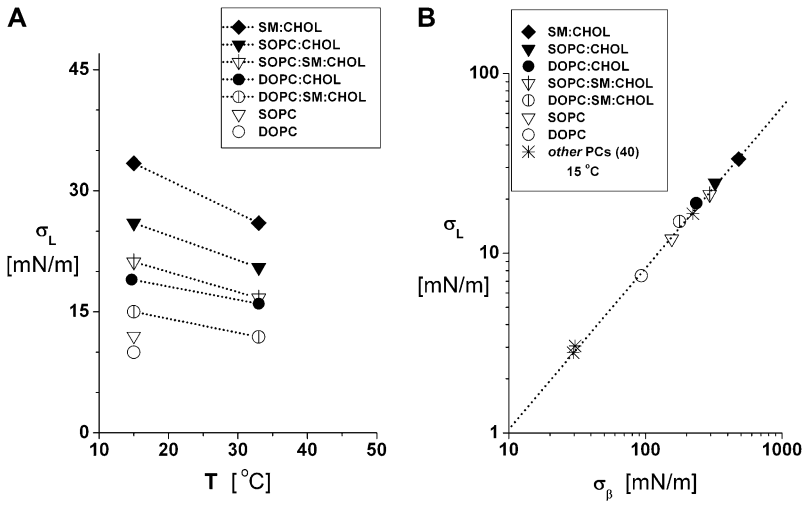

FIGURE 3 (*A*) Lysis tensions σ_L measured under continuous loading at 2 mN/m/s are plotted for temperatures of 15°C and 32–33°C for SOPC, 1:1 DOPC/CHOL, 1:1 SOPC/CHOL, 1:1 SM/CHOL, 1:1:1 DOPC/SM/CHOL, and 1:1:1 and 1:1:2 SOPC/SM/CHOL. Results for single-component SOPC and DOPC vesicles are plotted at 15°C. Fifty to eighty vesicles were tested for each system and temperature (means ± SD given in Table 1). Because membrane rupture is governed by kinetics, measurements of rupture tension have an inherent standard deviation (typically ~10−15%). However, the standard errors (standard error = standard deviation/$n^{1/2}$) in the measurements are smaller than the size of symbols in *A* for n ~50–80, which characterize the statistical uncertainties in the most frequent rupture events described by the nucleation theory given in the Appendix. (*B*) The lysis tensions obtained at 15°C are shown to correlate precisely with the values for thermal tension scale σ_β from fitting the kinetic model for rupture (as shown in the Appendix) to the stress-rate dependence of rupture tension.

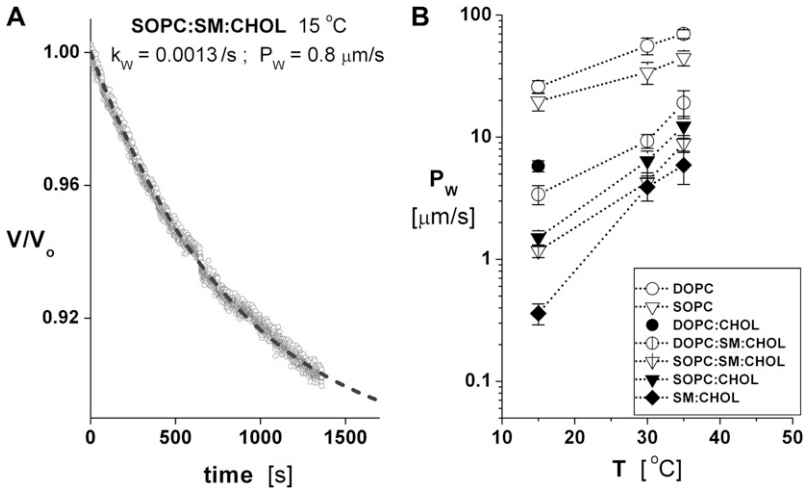

FIGURE 4 (*A*) Example of osmotic filtration from a 1:1:1 SOPC/SM/CHOL vesicle measured at 15°C after transfer from 205 mOsm solution to 236 mOsm. Superposed is the single parameter fit of the transport equation defined by the filtration rate k_W, which yields the coefficient P_W for water permeability. (*B*) Water permeabilities $P_W \pm$ SD measured at 15°C, 30°C, and 35°C for DOPC, SOPC, 1:1 SM/CHOL, 1:1 SOPC/CHOL, 1:1:1 DOPC/SM/CHOL, and 1:1:1 SOPC/SM/CHOL; 10–20 vesicles were tested for each system and temperature. Also plotted for comparison are water permeabilities for 1:1 DOPC/CHOL and 1:1:2 SOPC/SM/CHOL vesicles measured at 15°C.

were 30%–50% greater at the low tensions preceding a discontinuity than at high tensions above the discontinuity. Yet, when raised to 32–33°C or subjected to long periods of prestress (~1 mN/m) at the low temperature, the discontinuity in the elastic response disappeared. Elimination of the discontinuity in stretch resistance after long periods of prestress (or application of large tensions) suggests that mechanical stress acts to relieve some type of frustration in the microdomain structure produced during vesicle formation. Of related interest, downward breaks in the elastic responses of vesicles to tension have also been reported by Tierney et al. (44) for mixtures of dipalmitoylphosphatidylcholine (DPPC) and CHOL or ergosterol at low temperature. These authors attributed the discontinuous elastic response to disruption of a solid-like network of liquid-ordered and gel phases, producing a continuous liquid-ordered phase plus unconnected gel domains.

Driven to reach larger tensions by fast loading (i.e., σ_L ~15–20 mN/m at ~10 mN/m/s vis à vis σ_L ~10–12 mN/m at ~1 mN/m/s), the elastic responses of highly stretched PC bilayers expose a distinct curvature that agrees with predictions of a simple polymer theory introduced previously to describe the surface pressure of fluid acyl chains (35). Formulated in terms of the area strain (E. Evans and B. A. Smith, unpublished), $\sigma(\alpha_e) = 2\Pi_o[1 - g(\alpha_e,\varphi_c)/g(0, \varphi_c)]$, the model for tension-area response of PC lipids depends on a scale factor Π_o that defines the monolayer surface pressure at zero tension and a dimensionless function, $g(\alpha_e, \varphi_c)$, that characterizes the nonlinear strain dependence of the surface pressure. In addition to the surface pressure scale Π_o, the elastic-stretch response involves a geometric parameter, φ_c (<1), that characterizes the extent of lipid area condensation at zero tension relative to a state of maximum condensation ($\varphi_c = 1$). Although difficult to distinguish experimentally, different analytical expressions can be derived for $g(\alpha_e, \varphi_c)$ depending on how the lipid chains are modeled. As one example, the theory for freely jointed polymer chains yields the following expressions for the dimensionless surface pressure and elastic modulus: $g(\alpha_e, \varphi_c) = [(3 + 3\alpha_e - 2\varphi_c)/(1 + \alpha_e - \varphi_c)]/(1 + \alpha_e)^3$ and $K_A = 2\Pi_o \{3 + \varphi_c/[(1 - \varphi_c)(3 - 2\varphi_c)]\}$.

In earlier measurements the data for elastic stretch of PC bilayers loaded at ~1 mN/m/s were cut off by low rupture tensions and could be fit only by straight lines, as shown for a SOPC vesicle in Fig. 5 of Rawicz et al. (35), which resulted in values of K_A ~240 mN/m for SOPC and ~250 mN/m for DOPC (35). On the other hand, when SOPC and DOPC vesicles were stretched at tension rates of 10–100 mN/m/s, the measurements after correction for fluctuations overlayed precisely with the earlier tests in the regime of low tension but then revealed a prominent curvature as tensions continued to well above 10 mN/m. Low order polynomial (quadratic or cubic) fits to the full range of tensions for the SOPC and DOPC bilayers subjected to fast loading yield values of K_A ~290 ± 6 mN/m and 310 ± 20 mN/m, respectively. Most relevant here, with the improved video image analysis and corrections for thermal-bending fluctuations, it has been possible to account for the impact of curvature on the elastic stretch moduli of the phospholipid/CHOL systems since these bilayers break at large tensions even when loaded at ~1 mN/m/s (producing data sets containing several hundred points, as illustrated in Fig. 1). Consequently, although consistent with earlier studies demonstrating the major impact of CHOL on elasticity, the more precise measurements of area stretch with phospholipid/CHOL bilayers now yield elastic moduli that are twofold larger than those published in earlier reports (33,45). Interestingly, the larger moduli obtained for phospholipid/CHOL bilayers are closer in value to the area elastic moduli computed from recent atom-scale models of bilayers with similar constituents (46).

In regard to formation of domain structure, the nearest-neighbor interactions with CHOL work against the entropic elasticity of PC and SM acyl chains to condense the areas per molecule in these phospholipid/CHOL systems, as documented

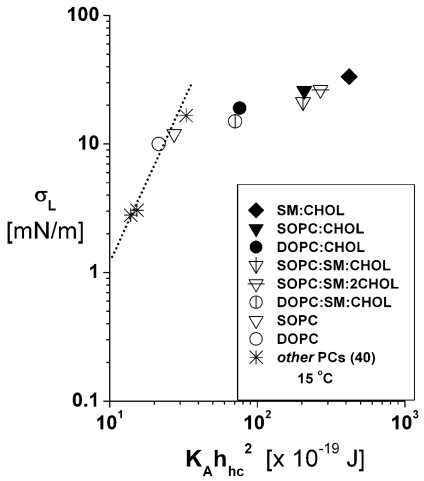

FIGURE 5 Lysis tensions σ_L measured at 15°C are plotted as functions of the bending elasticity parameter $K_A h_{hc}^2$ computed with the elastic-stretch moduli from Fig. 2 (Table 1) and values of hydrocarbon thickness in Table 2. Also included are data obtained previously for thin (diC13:0, diC18:2) and thick (diC22:1) PC bilayers (40). The dotted line connecting the data for the fluid PC bilayers indicates the correlation to bending elasticity expected for hydrophilic pores lined with rounded edges.

by NMR measurements of lipid chain order parameters (29,47–49). Furthermore, thermodynamic analysis of the elastic stretch responses measured for PC/CHOL bilayers shows that the interaction enthalpies for SOPC/CHOL and DOPC/CHOL interactions correlate with the measurements of elastic moduli (B. A. Smith and E. Evans, unpublished). Thus, characterizing the hierarchy of phospholipid-CHOL interactions, the values of K_A for the binary phospholipid/CHOL systems at 15°C were arrayed in the order SM/CHOL (~3300 mN/m) > SOPC/CHOL (~1980 mN/m) > DOPC/CHOL (~890 mN/m).

Unlike the two 18-carbon chains of SOPC and DOPC, brain SM contains a short saturated chain of sphingosine and a second chain formed primarily by either a saturated fatty acid or a long monounsaturated nervonic acid (C24:1). Also, the nervonic acid is expected to interact with CHOL much like a saturated hydrocarbon chain due to the relatively deep position of its double bond between carbons 15 and 16 (49,50). Hence, by avoiding an interaction between the steroid nucleus of CHOL and a *cis* double bond as would likely occur with oleoyl chains (C18:1), the energy of the SM-CHOL interaction is expected to be significantly greater than the energy of the SOPC-CHOL interaction (51–55). Accounting for the higher interaction energy, lipids with one or more saturated acyl chains (SM and SOPC) experience stronger van der Waals attraction to CHOL than do lipids with unsaturated (e.g., C18:1) chains. Concomitantly, increases in the distance between a saturated acyl chain and CHOL, as would occur with an increase in temperature, can markedly weaken this interaction. Thus, this weakening could account for the large temperature effect on the elastic moduli of the binary SM/CHOL, SOPC/CHOL, and ternary SOPC/SM/CHOL bilayers. By comparison, lipids such as DOPC containing symmetric C18:1 chains are likely to experience weaker van der Waals attraction to CHOL (51–55). Even so, the increased elastic resistance to area stretch of DOPC/CHOL bilayers compared to DOPC bilayers shows clearly that the interaction energy is not negligible. Consistent with the phase behavior deduced from other techniques (28,29), the competition between SM and PCs for CHOL most likely accounts for the differential effects of temperature on the elastic stretch moduli for the ternary 1:1:1 DOPC/SM/CHOL and 1:1:1 SOPC/SM/CHOL bilayers (Fig. 2).

Impact of stress on morphological evidence for domain structure

For all the bilayer systems tested at low (15°C) and high (33°C) temperatures, the small initial suction (~10 N/m^2 = 100 μAtm) used to capture each vesicle was sufficient to pressurize the vesicle segment outside the pipette into an optically perfect spherical shape. By comparison, in optical microfluorescence images (28,56–57), unstressed 1:1:1 PC/SM/CHOL vesicles have shown irregular morphologies at temperatures below 30°C that, over time, often formed large spherical ''bulges''. These bulges were not apparent in the shapes of the vesicles tested in our experiments (although the shapes of free SM/CHOL and PC/SM/CHOL vesicles were much less spherical and showed much slower fluctuations than for pure PC vesicles). The appearance and enlargement of bulges on raft microdomain-forming lipid vesicles have been attributed to a stress discontinuity along the domain boundaries (28,56–57). Modeled by a ''line tension'' γ (energy/length), the stress discontinuity at a domain boundary enables fluid domains with different mean curvatures to coexist in mechanical equilibrium. Incorporating other important aspects of membrane curvature elasticity, a recent detailed study of the vesicle shape mechanics (57) has shown that the magnitude of the line tensions in raft-containing lipid vesicles are small, with values ~1 pN. From simple first-order mechanics for a small spherical bulge on a large vesicle (radius R_v), it is easy to show that the aspect ratio for bulge height h_δ divided by the base radius r_δ of the bulge depends on the ratio of line tension to the level of vesicle pressurization P, i.e., $h_\delta/r_\delta \approx \gamma/(PR_v^2)$. Hence, for line tensions of ~1 pN, a small level of pressurization $P \sim 10$ N/m^2 is sufficient to reduce μm-size bulges on GUVs to below optical resolution (i.e., $h_\delta/r_\delta < 0.1$), which is consistent with the optically smooth spheres seen outside pipettes in our experiments.

Rupture strength

It is well known that bilayers composed of CHOL and phospholipids with saturated acyl chains are much stronger than the single-component fluid PC bilayers (33,45). Commensurate with this view, the lysis tensions measured here for

binary SM/CHOL and SOPC/CHOL as well as ternary 1:1:1 SOPC/SM/CHOL vesicles were found to be at least two- to threefold larger than for single-component SOPC bilayers. Less well appreciated, yet consistent with an appreciable energy of interaction, the addition of CHOL was found here to also significantly strengthen bilayers composed of symmetrically unsaturated DOPC (e.g., at 15°C, σ_L increased from ~10 mN/m for DOPC to 19 mN/m for 1:1 DOPC/CHOL). The rupture tensions for all the phospholipid/CHOL bilayer systems (Fig. 3 *A*) were found to decrease by ~20% as the temperature was increased from 15°C to 33°C.

The possible connection between bilayer strength and elasticity (in particular, the area compressibility $1/K_A$) has been suggested for some time (33,45). The underlying concept is that the formation of a ''rupture pore'' in a bilayer involves significant elastic deformation of the lipid monolayers. However, when corrected for thermal-bending fluctuations, there is little variation between measurements of the area elastic moduli for different fluid phase PC bilayers (35) while at the same time the rupture tensions vary significantly in a manner that depends strongly on chain length (40). Supporting the paradigm that pores in PC bilayers are rounded and lined with lipid headgroups to reduce exposure of hydrocarbon to water, the rupture strengths of fluid PC bilayers appear to correlate with the square of the elastic-bending moduli (40). Since the bending modulus scales as the product of area-stretch modulus and square of the deformable-hydrocarbon thickness, i.e., $\sim K_A h_{hc}^2$ (35), the elastic-stretch moduli measured at 15°C (Fig. 2) and values of the deformable hydrocarbon thicknesses h_{hc} derived from x-ray measurements (listed in Table 2) were used to characterize the bending stiffnesses of all the lipid and lipid/CHOL systems. Fig. 5 shows the comparison between rupture tensions and bending stiffnesses measured in this study along with the data reported previously for other fluid PC bilayers (40). As seen in Fig. 5, the phospholipid/CHOL systems depart significantly from the strong dependence on bending stiffnesses exhibited by the strengths of single-component PC bilayers.

TABLE 2 Bilayer thickness measurements

System	h_{pp} (nm)	$h_{hc} \approx h_{pp} - 1$ (nm)
DOPC	3.64 ± 0.1	2.64
SOPC	4.07 ± 0.06	3.07
1:1 DOPC/CHOL	~4.0 ± 0.1	~3
1:1:1 DOPC/SM/CHOL	4.30 ± 0.15	3.3
1:1:1 SOPC/SM/CHOL	4.45 ± 0.07	3.45
1:1 SOPC/CHOL	4.24 ± 0.05	3.24
1:1 SM/CHOL	4.55 ± 0.06	3.55

Measurements of average bilayer peak-peak headgroup distances (h_{pp}) in multilamellar arrays at 20°C obtained by x-ray diffraction. Data for 1:1 SOPC/CHOL and 1:1:1 SOPC/SM/CHOL are from this study. Data for DOPC, SOPC, 1:1:1 DOPC/SM/CHOL, and 1:1 SOPC/CHOL are taken from Gandhavadi et al. (9), McIntosh et al. (34), and Rawicz et al. (35). For 1:1 DOPC/CHOL, an estimate of thickness was made by using the value of $h_{pp} = 3.8$ nm measured previously for 2:1 DOPC/CHOL (9). A deformable hydrocarbon thickness h_{hc} was estimated for each system by subtracting ~1 nm for headgroup dimensions from the peak-peak headgroup separation.

Water permeability

Similar to the impact of CHOL on elastic moduli and rupture strengths, addition of CHOL to bilayers made from PC lipids dramatically reduced the permeability of vesicles to water in our tests, as found in earlier work (45,58). Limited mainly by the small solubility of water in the hydrocarbon interior (43,59), bilayer permeability is expected to depend strongly on the creation of ''free volume'' in the hydrocarbon region driven by thermal fluctuations in acyl chain packing. Even though PC bilayers have nearly the same lipid-area-stretch moduli, the free volume is expected to increase exponentially with increase in the reduced temperature relative to the gel-liquid crystalline phase transition, which seems to account for the variations in PC bilayer permeability associated with different chain lengths and levels of unsaturation (38). However, the results in Fig. 6 show a distinct correlation between water permeability and area compressibility for the binary and ternary phospholipid/CHOL systems that differs significantly from the single-component PC bilayers. Perhaps accounting for correlation among the CHOL-containing systems, recent molecular simulations have demonstrated that the free volume in phospholipid/CHOL bilayers increases with increase in the area compressibility (60,61).

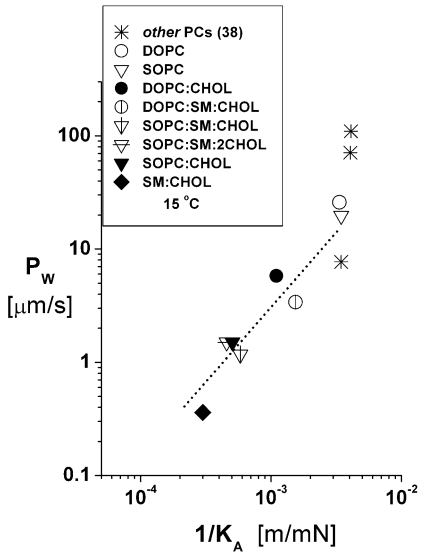

FIGURE 6 Values of water permeability P_W measured at 15°C are plotted as functions of the area compressibility $1/K_A$ as defined by the elastic-stretch moduli at 15°C in Fig. 2 (Table 1). Also included are data for other fluid-PC bilayers (taken from Rawicz et al. (35) and Olbrich et al. (38)). The dashed-dotted line was added to highlight the correlation between permeability and area compressibility among the phospholipid/CHOL systems.

Most intriguing, a striking correlation was obtained between the logarithm of water permeability and the bilayer lysis tension for all the single-component PC and phospholipid/CHOL systems (Fig. 7). This outcome suggests that fluctuations in acyl chain conformations not only regulate water partitioning inside bilayers but are also an important factor governing the rare defects that nucleate rupture pores. As notable exceptions to the correlation in Fig. 7, the ternary 1:1:1 PC/SM/CHOL systems are of particular interest because they have been previously shown to contain microdomains (25–29). Surprisingly, these systems appear much less permeable to water than predicted by their lysis tensions (Fig. 7), seeming to rule out appreciable water leakage at domain boundaries. Significantly, when the CHOL fraction is increased, the ternary 1:1:2 SOPC/SM/CHOL system is seen to also agree with the correlation between the logarithm of permeability and lysis tension (falling just behind the data point for 1:1 SOPC/CHOL in Fig. 7). Based on what we know about the phase diagrams for ternary phospholipid/CHOL systems (28,29), increasing the CHOL content from 1:1:1 PC/SM/CHOL to 1:1:2 PC/SM/CHOL would move the system toward a single liquid-phase miscibility region, leading to solubilization of the microdomain structure. Still, the cause of deviations of the 1:1:1 PC/SM/CHOL systems from the correlation shown in Fig. 7 are not clear since they could arise from either anomalous reductions in the permeability to water or in the lysis tensions or both.

CONCLUSION

The micromechanical tests described in this work show the important role of PC, SM, and CHOL composition in determining the elasticity, strength, and water permeability of vesicle bilayers. In addition to PC hydrocarbon-chain unsaturation, the mechanical-stress history and temperature are important factors determining the strength and permeation properties of the ternary bilayer systems shown in previous studies to contain raft microdomains.

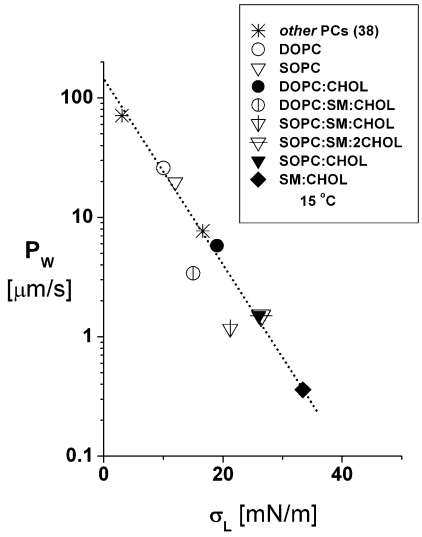

FIGURE 7 Values of water permeability P_W measured at 15°C are plotted versus the lysis tensions σ_L measured at 15°C.

APPENDIX

It is well established from studies of voltage-dependent conductance fluctuations in planar bilayers that small pore-like defects appear frequently in membranes and quickly collapse. Likewise, as recognized many years ago (62), the dielectric breakdown of a thin fluid film requires the creation of an extremely rare pore that is mechanically unstable under the film tension. By analogy to cavity formation in a three-dimensional fluid, the energetic barrier characterizing this metastable event is derived from the maximum in the total energy needed to create the pore structure minus the mechanical work contributed by the tension times increase in area of the membrane. Given a constant energy per perimeter length of the pore (''edge energy'' ε), the energy barrier for a circular hole is approximated by $E_{\text{hole}} \approx \pi\varepsilon^2/\sigma$, with the area of the critical-size hole defined by $-\partial E_{\text{hole}}/\partial\sigma \approx \pi(\varepsilon/\sigma)^2$. Because the energy barrier is usually very large, thermal activation is needed to assist nucleation of an unstable pore. Based on the classical Kramers-Smoluchowski theory for kinetics in overdamped (Brownian) systems, the frequency of pore nucleation $\nu_{\text{rup}}(\sigma)$ is shown to be dominated by a tension-dependent Arrhenius factor, $\exp[-(\pi\varepsilon^2/k_BT)/\sigma]$, which defines the thermal scale for rupture tension, $\sigma_\beta = \pi\varepsilon^2/k_BT$. The frequency for pore nucleation involves a prefactor (attempt rate) ν_h^o proportional to the ratio of σ_β to the viscous coefficient for damping of hole excitations and a modest dependence on tension (40) as expressed by

$$\nu_{\text{rup}}(\sigma) \approx \nu_h^o(\sigma/\sigma_\beta)^{1/2}\exp(-\sigma_\beta/\sigma)$$

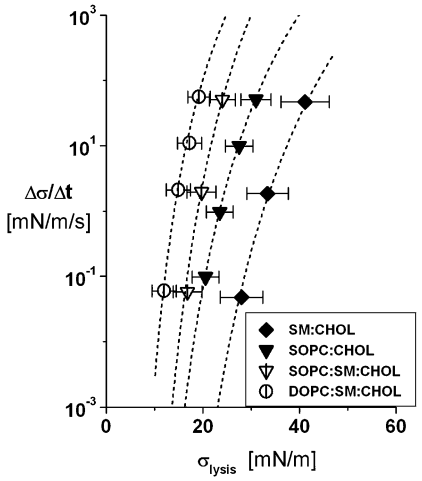

FIGURE 8 Stress-rate dependences of the lysis tensions measured at 15°C for the ternary 1:1:1 PC/SM/CHOL plus binary 1:1 SM/CHOL and 1:1 PC/CHOL vesicles. Here, the standard deviations in rupture tensions are added to show the inherent widths in distributions of rupture events that arise from the kinetics of membrane failure. As noted in the legend of Fig. 3, very small standard errors in measurements represent the relevant statistical variations that characterize the most frequent rupture events. (Even though similar in form, the results for 1:1 DOPC/CHOL and 1:1:2 SOPC/SM/ CHOL vesicles were left out of the figure for clarity.) The continuous dotted curves are fits of the kinetic rupture model described in the Appendix to the most frequent rupture tensions yielding the thermal tension scales σ_β correlated with the single stress-rate measurements of lysis tension plotted in Fig. 3 *B*.

If held at constant tension, the probability of membrane survival, $S(t) = \exp[-\int_{o\to t}\nu_{rup}(y)dy]$, is a simple exponential decay over time, $S(t) = \exp[-\nu_{rup}(\sigma)t]$, with the mean lifetime given by, $\tau_{rup} = 1/\nu_{rup}(\sigma)$. On the other hand, when the membrane is subjected to a tension ramp, $\sigma = r_\sigma t$, the frequency of rupture pore nucleation increases rapidly in time. At a fixed stress rate r_σ, the probability of membrane survival to a particular level of tension is found directly from the survival over time (40), $S(\sigma) = \exp[-(1/r_\sigma)\int_{o\to\sigma}\nu_{rup}(y)dy]$, which predicts the following distribution (statistics) of rupture tensions: $p(\sigma) = [\nu(\sigma)/r_\sigma]S(\sigma)$. Although the form of this distribution is easily computed numerically, what is most useful for experimental analysis is the simple analytical expression that describes the ''most frequent lysis'' (MFL) tension σ_L as a function of stress rate. Defining membrane strength, the MFL event is the maximum (peak) in the distribution, $\partial p(\sigma)/\partial\sigma = 0$, which relates the stress rate r_σ to the change (derivative) of lifetime $(1/\nu_{rup})$ with change in tension, i.e., $1/r_\sigma = -\partial\tau_{rup}(\sigma)/\partial\sigma|_{MFL}$. Using the kinetic model for the lifetime as a function of tension, $\tau_{rup}(\sigma) \approx (\sigma_\beta/\sigma)^{1/2}\exp(\sigma_\beta/\sigma)/\nu_h^o$, we obtain a transcendental expression relating lysis tension σ_L to the stress rate, $\sigma_\beta/\sigma_L \approx 5/2\, log_e(\sigma_L/\sigma_\beta) - \log_e[r_\sigma/(\nu_h^o\sigma_\beta)]$, as noted in the text. The results plotted in Fig. 8 demonstrate that this equation closely matches the stress-rate dependences of the lysis tensions measured for ternary 1:1:1 PC/SM/CHOL and binary 1:1 SM/CHOL plus 1:1 PC/CHOL vesicles. (For clarity, the results for 1:1 DOPC/CHOL and 1:1:2 SOPC/SM/CHOL vesicles were left out of Fig. 8 because they overlap with the data for 1:1:1 SOPC/SM/CHOL.)

This work was supported by grants FRN-7477 from the Canadian Institutes of Health Research (to E.E.), HL65333 (to E.E.), and GM27278 (to T.J.M.) from the National Institutes of Health, and from Philip Morris International and Philip Morris (to S.A.S.).

REFERENCES

1. Keenan, T. W., and D. J. Morre. 1970. Phospholipid class and fatty acid composition of Golgi apparatus isolated from rat liver and comparison with other cell fractions. *Biochemistry.* 9:19–25.
2. Fridriksson, E. K., P. A. Shipkova, E. D. Sheets, D. Holowka, B. Baird, and F. W. McLafferty. 1999. Quantitative analysis of phospholipids in functionally important membrane domains from RBL-2H3 mast cells using tandem high-resolution mass spectrometry. *Biochemistry.* 38: 8056–8063.
3. Yorek, M. A. 1993. Biological distribution. *In* Phospholipids Handbook. G. Cevc, editor. Marcel Dekker, New York. 745–775.
4. Simons, K., and E. Ikonen. 1997. Functional rafts in cell membranes. *Nature.* 387:569–572.
5. Brown, D. A., and E. London. 1998. Functions of lipid rafts in biological membranes. *Annu. Rev. Cell Dev. Biol.* 14:111–136.
6. Brown, D. A., and E. London. 2000. Structure and function of sphingolipid- and cholesterol-rich membrane rafts. *J. Biol. Chem.* 275: 17221–17224.
7. Gkantiragas, I., B. Brugger, E. Stuven, D. Kaloyanova, X.-Y. Li, K. Lohr, F. Lottspeich, F. T. Wieland, and J. B. Helms. 2001. Sphingomyelin-enriched microdomains at the Golgi complex. *Mol. Biol. Cell.* 12:1819–1833.
8. Ahmed, S. N., D. A. Brown, and E. London. 1997. On the origin of sphingolipid/cholesterol-rich detergent-insoluble cell membranes: physiological concentrations of cholesterol and sphingolipid induce formation of a detergent-insoluble, liquid-ordered lipid phase in model membranes. *Biochemistry.* 36:10944–10953.
9. Gandhavadi, M., D. Allende, A. Vidal, S. A. Simon, and T. J. McIntosh. 2002. Structure, composition, and peptide binding properties of detergent soluble bilayers and detergent resistant rafts. *Biophys. J.* 82:1469–1482.
10. Young, R. M., D. Holowka, and B. Baird. 2003. A lipid raft environment enhances Lyn kinase activity by protecting the active site tyrosine from dephosphorylation. *J. Biol. Chem.* 278:20746–20752.
11. Arni, S., S. A. Keilbaugh, A. G. Ostermeyter, and D. A. Brown. 1998. Association of GAP-43 with detergent-resistant membranes requires two palmitoylated cysteine residues. *J. Biol. Chem.* 273:28478–28485.
12. Melkonian, K. A., A. G. Ostermeyer, J. Z. Chen, M. G. Roth, and D. A. Brown. 1999. Role of lipid modifications in targeting proteins to detergent-resistant membrane rafts. Many raft proteins are acylated, while few are prenylated. *J. Biol. Chem.* 274:3910–3917.
13. Moffett, S., D. A. Brown, and M. E. Linder. 2000. Lipid-dependent targeting of G proteins into rafts. *J. Biol. Chem.* 275:2191–2198.
14. Benting, J., A. Rietveld, I. Ansorge, and K. Simons. 1999. Acyl and alkyl chain length of GPI-anchors is critical for raft association in vitro. *FEBS Lett.* 462:47–50.
15. Sharma, P., R. Varma, R. C. Sarasij, Ira, K. Gousset, G. Krishnamoorthy, M. Rao, and S. Mayor. 2004. Nanoscale organization of multiple GPI-anchored proteins in living cell membranes. *Cell.* 116:577–589.
16. Field, K. A., D. Holowka, and B. Baird. 1997. Compartmentalized activation of the high affinity immunoglobulin E receptor within membrane domains. *J. Biol. Chem.* 272:4276–4280.
17. Ridyard, M. S., and S. M. Robbins. 2003. Fibroblast growth factor-2-induced signaling through lipid raft-associated fibroblast growth factor receptor substrate 2 (FRS2). *J. Biol. Chem.* 278:13803–13809.
18. Schubert, A. L., W. Schubert, D. C. Spray, and M. P. Lisanti. 2002. Connexin family members target to lipid raft domains and interact with caveolin-1. *Biochemistry.* 41:5754–5764.
19. Wong, W., and L. C. Schlichter. 2004. Differential recruitment of Kv1.4 and Kv4.2 to lipid rafts by PSD-95. *J. Biol. Chem.* 279:444–452.
20. Ishikawa, Y., Z. Yuan, N. Inoue, M. T. Skowronski, Y. Nakae, M. Shono, G. Cho, M. Yasui, P. Agre, and S. Nielsen. 2005. Identification of aquaporin-5 in lipid rafts and its translocation to apical membranes by the activation of M3-muscarinic acetylcholine receptors in the interlobular ducts of rat parotid glands. *Am J Physiol Cell Physiol.* 289:C1303–C1311.
21. Simons, K., and D. Toomre. 2000. Lipid rafts and signal transduction. *Nat. Rev. Mol. Cell Biol.* 1:31–39.
22. Simons, K., and G. van Meer. 1988. Lipid sorting in epithelial cells. *Biochemistry.* 27:6197–6202.
23. Simons, K., and E. Ikonen. 2000. How cells handle cholesterol. *Science.* 290:1721–1726.
24. Ikonen, E. 2001. Roles of lipid rafts in membrane transport. *Curr. Opin. Cell Biol.* 13:470–477.
25. Rinia, H. A., and B. deKruijff. 2001. Imaging domains in model membranes with atomic force microscopy. *FEBS Lett.* 504:194–199.
26. Dietrich, C., L. A. Bagatolli, Z. N. Volovyk, N. L. Thompson, M. Levi, K. Jacobson, and E. Gratton. 2001. Lipid rafts reconstituted in model membranes. *Biophys. J.* 80:1417–1428.
27. Samsonov, A. V., I. Mihalyov, and F. S. Cohen. 2001. Characterization of cholesterol-sphingomyelin domains and their dynamics in bilayer membranes. *Biophys. J.* 81:1486–1500.
28. Veatch, S. L., and S. L. Keller. 2003. Separation of liquid phases in giant vesicles of ternary mixtures of phospholipids and cholesterol. *Biophys. J.* 85:3074–3083.
29. Veatch, S. L., I. V. Polozov, K. Gawrisch, and S. L. Keller. 2004. Liquid domains in vesicles investigated by NMR and fluorescence microscopy. *Biophys. J.* 86:2910–2922.
30. Lundbaek, J. A., O. S. Andersen, T. Werge, and C. Nielsen. 2003. Cholesterol-induced protein sorting: an analysis of energetic feasibility. *Biophys. J.* 84:2080–2089.
31. McIntosh, T. J., A. Vidal, and S. A. Simon. 2003. Sorting of lipids and transmembrane peptides between detergent-soluble bilayers and detergent-resistant rafts. *Biophys. J.* 85:1656–1666.
32. Vidal, A., and T. J. McIntosh. 2005. Transbilayer peptide sorting between raft and nonraft bilayers: comparisons of detergent extraction and confocal microscopy. *Biophys. J.* 89:1102–1108.

33. Needham, D., and R. S. Nunn. 1990. Elastic deformation and failure of lipid bilayer membranes containing cholesterol. *Biophys. J.* 58:997–1009.

34. McIntosh, T. J., S. A. Simon, D. Needham, and C.-h. Huang. 1992. Structure and cohesive properties of sphingomyelin:cholesterol bilayers. *Biochemistry.* 31:2012–2020.

35. Rawicz, W., K. C. Olbrich, T. McIntosh, D. Needham, and E. Evans. 2000. Effect of chain length and unsaturation on elasticity of lipid bilayers. *Biophys. J.* 79:328–339.

36. McMullen, T. P. W., R. N. A. H. Lewis, and R. N. McElhaney. 2004. Cholesterol-phospholipid interactions, the liquid-ordered phase and lipid rafts in model and biological membranes. *Curr. Opin. Colloid Interface Sci.* 8:459–468.

37. Hinderliter, A., R. L. Biltonen, and P. F. Almeida. 2004. Lipid modulation of protein-induced membrane domains as a mechanism for controlling signal transduction. *Biochemistry.* 43:7102–7110.

38. Olbrich, K., W. Rawicz, D. Needham, and E. Evans. 2000. Water permeability and mechanical strength of polyunsaturated lipid bilayers. *Biophys. J.* 79:321–327.

39. Evans, E. A., and W. Rawicz. 1990. Entropy-driven tension and bending elasticity in condensed-fluid membranes. *Phys. Rev. Lett.* 64: 2094–2097.

40. Evans, E., V. Heinrich, F. Ludwig, and W. Rawicz. 2003. Dynamic tension spectroscopy and strength of biomembranes. *Biophys. J.* 85: 2342–2350.

41. Heinrich, V., and W. Rawicz. 2005. Automated, high-resolution micropipet aspiration reveals new insight into the physical properties of fluid membranes. *Langmuir.* 21:1962–1971.

42. Evans, E., and F. Ludwig. 2000. Dynamic strengths of molecular anchoring and material cohesion in fluid biomembranes. *J. Phys. Condens. Matter.* 12:A315–A320.

43. Finkelstein, A. 1976. Water and nonelectrolyte permeability of lipid bilayer membranes. *J. Gen. Physiol.* 68:127–135.

44. Tierney, K. J., D. E. Block, and M. L. Longo. 2005. Elasticity and phase behavior of DPPC membrane modulated by cholesterol, ergosterol, and ethanol. *Biophys. J.* 89:2481–2493.

45. Bloom, M., E. Evans, and O. G. Mouritsen. 1991. Physical properties of the fluid lipid-bilayer component of cell membranes: a perspective. *Q. Rev. Biophys.* 24:293–397.

46. Niemela, P. S., S. Ollila, M. T. Hyvonen, M. Karttunen, and I. Vattulainen. 2007. Assessing the nature of lipid raft membranes. *PloS Comput. Biol.* 3:0304–0312.

47. Lafleur, M., P. R. Cullis, and M. Bloom. 1990. Modulation of the orientational order profile of the lipid acyl chain in the L_α phase. *Eur. Biophys. J.* 19:55–62.

48. Henriksen, J., A. C. Rowat, E. Brief, Y. W. Hsueh, J. L. Thewalt, M. J. Zuckermann, and J. H. Ipsen. 2006. Universal behavior of membranes with sterols. *Biophys. J.* 90:1639–1649.

49. Bunge, A., P. Müller, M. Stöckl, A. Herrmann, and D. Huster. 2008. Characterization of the ternary mixture of sphingomyelin, POPC, and cholesterol. Support for an inhomogeneous lipid distribution at high temperatures. *Biophys. J.* 94:2680–2690.

50. Smaby, J. M., H. L. Brockman, and R. E. Brown. 1994. Cholesterol's interfacial interactions with sphingomyelins and phosphatidylcholines: hydrocarbon chain structure determines the magnitude of condensation. *Biochemistry.* 33:9135–9142.

51. Ramstedt, B., and J. P. Slotte. 1999. Interaction of cholesterol with sphingomyelins and acyl-chain-matched phosphatidylcholines: a comparative study of the effect of the chain length. *Biophys. J.* 76: 908–915.

52. Lund-Katz, S., H. M. Laboda, L. R. McLean, and M. C. Phillips. 1988. Influence of molecular packing and phospholipid type on rates of cholesterol exchange. *Biochemistry.* 27:3416–3423.

53. Pandit, S. A., E. Jakobsson, and H. L. Scott. 2004. Simulation of the early stages of nano-domain formation in mixed bilayers of sphingomyelin, cholesterol, and dioleylphosphatidylcholine. *Biophys. J.* 87: 3312–3322.

54. Czub, J., and M. Baginski. 2006. Comparative molecular dynamics study of lipid membranes containing cholesterol and ergosterol. *Biophys. J.* 90:2368–2382.

55. Sankaram, M. B., and T. E. Thompson. 1990. Interaction of cholesterol with various glycerophospholipids and sphingomyelin. *Biochemistry.* 29:10670–10675.

56. Baumgart, T., S. T. Hess, and W. W. Webb. 2003. Imaging coexisting fluid domains in biomembrane models coupling curvature and line tension. *Nature.* 425:821–824.

57. Baumgart, T., S. Das, W. W. Webb, and J. T. Jenkins. 2005. Membrane elasticity in giant vesicles with fluid phase coexistence. *Biophys. J.* 89:1067–1080.

58. Blok, M. C., L. L. Van Deenen, and J. De Gier. 1977. The effect of cholesterol incorporation on the temperature dependence of water permeation through liposomal membranes prepared from phosphatidylcholines. *Biochim. Biophys. Acta.* 464:509–518.

59. Carruthers, A., and D. L. Melchior. 1983. Study of the relationship between bilayer water permeability and bilayer physical state. *Biochemistry.* 22:5797–5807.

60. Marrink, S. J., R. M. Sok, and H. J. C. Berendsen. 1996. Free volume properties of simulated lipid membrane. *J. Chem. Phys.* 104:9090–9099.

61. Falck, E., M. Patra, M. Karttunen, M. T. Hyvonen, and I. Vattulainen. 2004. Lessons of slicing membranes: interplay of packing, free area, and lateral diffusion in phospholipid/cholesterol bilayers. *Biophys. J.* 87:1076–1091.

62. Deryagin, B. V., and Y. V. Gutop. 1962. Theory of the breakdown (rupture) of free films. *Kolloidn. Zh.* 24:370–374.